Z. Physik C, Particles and Fields 7, 357–371 (1981)

Zeitschrift für Physik C Particles and Fields

Regge Cuts and Neutral Pion Electroproduction

P. D. B. Collins and T. D. B. Wilkie

Physics Department, University of Durham, Durham City DH1 3LE, England

Received 29 September 1980

Abstract. A complete FESR-plus-Regge analysis is made of neutral pion photoproduction and electroproduction to understand the Regge cut and its dependence on k^2, the square of the virtual photon mass. A SCRAM type of model is essential, but contrary to previous expectations the range of the photon-proton interaction which gives rise to the cut increases with $-k^2$, and is not related to the pointlike, scaling behaviour of deep inelastic scattering, which arises from much simpler parton-model diagrams.

1. Introduction

In the late 1960's and early 1970's two conflicting explanations of the dip structures found in differential cross sections were fashionable. According to one viewpoint [1–3] the coincidence of some of these dips with the points in t where the exchanged Regge trajectories $\alpha(t)$ passed through nonsense values demonstrated that the dips were nonsense wrong-signature zeros (NWZ) of the Regge pole amplitudes, $A \sim \alpha(t)$, and weak Regge cuts would modify these dips only slightly [3]. The best known example is of course the dip in $\frac{d\sigma}{dt}(\pi^- p \to \pi^\circ n)$ at $-t \approx 0.5\,\mathrm{GeV}^2$ where $\alpha_\varrho(t)=0$. The alternative view was that the Reggeons themselves are essentially featureless as functions of t, and the dips are analagous to diffraction minima caused by the destructive interference between the poles and strong absorbtive Regge cuts (the SCRAM model, [4, 5]). The resulting amplitudes take the form [6]

$$A \sim J_n(R\sqrt{-t}) \tag{1.1}$$

where $J_n(x)$ is a Bessel function, R is the effective radius of interaction, and n the net change of helicity. In the $\pi^- p \to \pi^\circ n$ example the dominant $n=1$ amplitude has a zero at $-t \approx 0.5$ GeV^2 if $R \approx 1$ fm, due to the vanishing of the Bessel function at $x=3.83$. This latter view has been admirably summarized and fitted to an impressive array of data by Kane and Seidl [5]. But because of the continuation of Regge-pole shrinkage to large $|t|$, and the lack of a fundamental theoretical foundation for the absorption idea which is central to the SCRAM model, for most observers the problem remains unresolved (see [7, 8] for surveys).

In 1971 Harari [9] suggested an ingenious way in which the argument might be settled experimentally. He noted that in $\gamma p \to \pi^\circ p$ there is a dip in the differential cross section at $|t|=0.5$ GeV^2. From one view (NWZ) this is due to the dominant ω exchange trajectory passing through $\alpha_\omega(t)=0$, while from the other (SCRAM) it stems from the cancellation of the ω pole by an absorptive $\omega \otimes P$ cut ($P \equiv$ pomeron) in the predominant single-flip helicity amplitude. Both views thus account qualitatively for the basic facts, and even fairly quantitatively (compare [10–14]). However, if one considers instead neutral-pion electroproduction, effectively $\gamma_v(k^2)p \to \pi^0 p$ where $k^2(<0)$ is the square of the virtual photon's mass, the two models will not necessarily make identical predictions. If the dip is a nonsense zero its position should remain fixed in t since the structure of the ω-exchange amplitude should be independent of the external masses, but if an absorptive cut is responsible it seems quite likely that the dip position (in t) will move with $-k^2$ since the range over which the absorption mechanism operates may well change.

Harari argued that the range of interaction, R, between the spacelike photon and the proton should decrease with increasing $-k^2$. This is because a more highly virtual photon can exist only for a shorter period of time, and so the effective radius within which virtual hadronic matter can be created should decrease [15, 16]. Old-fashioned perturbation theory leads one to expect that in the target proton's rest frame the distance over which a virtual hadronic component of

0170-9739/81/0007/0357/$03.00

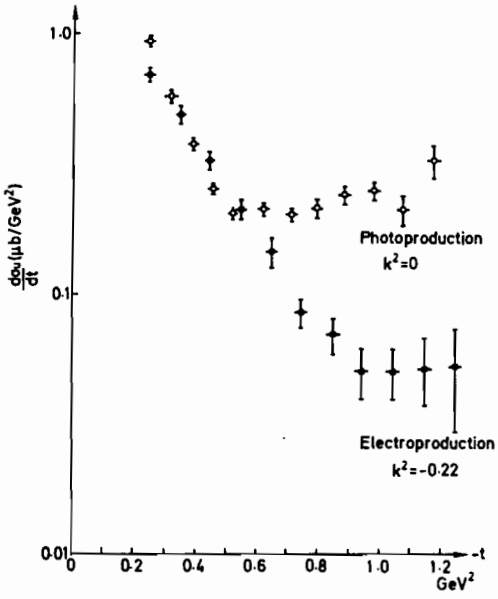

Fig. 1. Comparison of electroproduction $\frac{d\sigma}{dt}$ at $s=6.5$ GeV² and $k^2=-0.22$ GeV² with photoproduction, from [22]. The disappearance of the secondary maximum is evident

the photon with mass M will propagate is given by [17]

$$R=\frac{2|k|}{M^2-k^2} \tag{1.2}$$

where k_μ is the photon's four momentum. The success of the vector dominance model [18] (VDM) suggests that one should take $M^2\approx m_\varrho^2$. Clearly if R does decrease in this sort of way the position of the zero of $J_1(R\sqrt{-t})$ will occur at larger values of $\sqrt{-t}$ as $-k^2$ increases, i.e. the dip should move out to larger angles. Similarly Frass et al. [19] have shown that one would expect the photon to shrink with $-k^2$ in the generalized vector dominance model. Unfortunately the tests that this shrinkage does occur, e.g. in $\gamma p\to Vp$ ($V=\varrho^0, \phi$) are rather ambiguous [20].

Experiments were performed on π^0 electroproduction to try and test Harari's hypothesis, the first data appearing in 1975 [21] and further work in 1978 [22]. The results, illustrated in Fig. 1, confounded all expectations, since the dip neither remained fixed nor moved out with $-k^2$ but simply disappeared as k^2 was changed from 0 to -0.22 GeV². In electroproduction even for comparatively small $-k^2$ the data continue to fall with $-t$ beyond the photoproduction dip. But in other respects, such as the $\left(1-\frac{k^2}{m_\varrho^2}\right)^{-1}$ VDM dependence of the forward peak and the dominance of natural parity exchange, the virtual photon is still behaving like a hadron in this process.

Not surprisingly there have been rather few published attempts to explain this odd behaviour. Vanryckeghem [23] used the photoproduction Regge fit of Barker et al. [14] and extended it to electroproduction by giving an anomalous k^2 dependence to a low-lying, and rather unphysical, effective trajectory. Later Barker and Storrow [24] tried to explain the data by a k^2 dependence of their Regge cut residues, but they were not able to account satisfactorily for the sharp change of t dependence between $k^2=0$ and $k^2=-0.22$ GeV². There is unfortunately a good deal of ambiguity because the electroproduction data are available at only one rather low energy ($s=6.5$ GeV²) and heavy reliance must be placed on the hypothesis that the energy dependence of electroproduction is similar to that of photoproduction.

However, there is also quite good data on low-energy resonance excitation in electroproduction. It has often proved fruitful in the past to combine Regge fits of high-energy data with finite-energy-sum-rule (FESR) evaluations of low-energy data [7], thus extending the effective energy range of the data and making use of the phase information contained in phase-shift analyses. This was done by Barker et al. [14] for example in their work on π^0 photoproduction. There have been several indications, both from the experimental data [25] and quark-model calculations [26, 27], that some resonances behave quite differently from in photoproduction, and it is obviously interesting to see if the electroproduction FESR exhibit an anomalous behaviour similar to the high-energy cross section.

The purpose of this paper is to report a complete FESR plus Regge analysis of all the data on π^0 photoproduction and electroproduction in an attempt to understand why electroproduction behaves so strangely.

In the next section we review a Regge pole and cut fit of high energy $\gamma p\to\pi^0 p$ and related processes made previously [13], and consider the modifications which are necessary to bring it into accord with the FESR over the resonance region. Armed with this knowledge we then apply the same methods to the electroproduction data in Sect. 3, demanding continuity in k^2. To achieve this we must deploy a good deal of formalism to relate the amplitudes conventionally employed in photo and electro-production, and especially to obtain the contribution of resonance multipoles, with their form factors, to the helicity amplitudes. We have gathered the main features of this formalism into the appendix. Our conclusions are given in the final section.

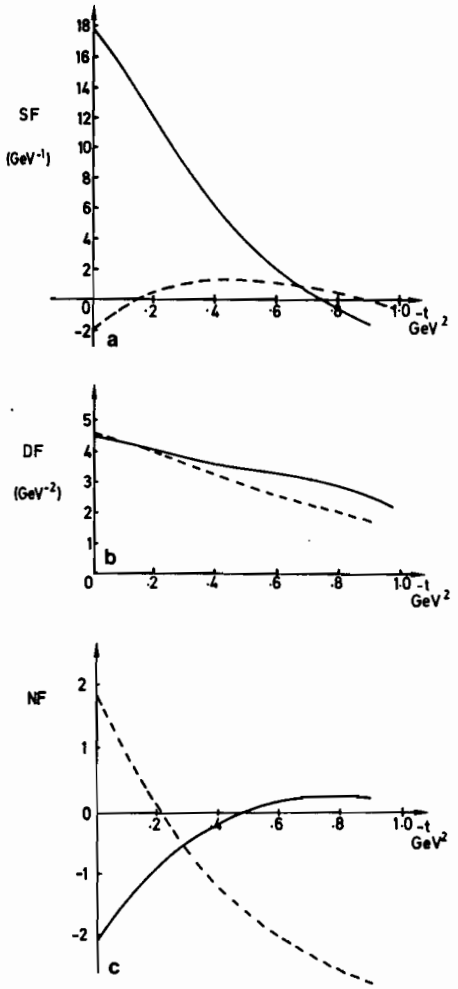

Fig. 2a—c. The photoproduction FESR integrals. The dashes are the integral (2.7) of the Regge amplitude and the solid curves are the integral (2.8) of the resonances for **a** the single-flip amplitude, **b** the double flip amplitude **c** the non-flip amplitude

Table 1. The Regge pole and cut parameters of the fit to the photoproduction data using (2.1)–(2.6)

	ϱ	ω	P	f
$\alpha(0)$	0.57	0.39	1.0	0.55
α'	0.72	1.01	0.49	1.1
G_{++}	0.504	10.75		
G_{+-}	1.23	7.37		
a_{++}	4.42	1.07		
a_{++}	0.02	1.61		
λ_0	2.88	1.51		
λ_1	2.93	2.89		
λ_2	2.70	1.65		
σ_T			51.17	
E_0				−111.25
h			2.02	0.23

All these parameters are in GeV units. (Given the change of units and the use of G_{++}, G_{+-} instead G_T and G_V these are essentially identical to the parameters of [13])

2. Neutral Pion Photoproduction

a) The Regge Fit

A good economical fit to the high-energy data on $\gamma p \to \pi^0 p$, $\gamma n \to \pi^0 n$ and $\gamma p \to \eta p$ can be obtained with just the ω and ϱ trajectory exchanges modified by strong cuts, calculated as in the SCRAM absorbtion model, but incorporating both P (pomeron) and f exchanges in the final-state interaction [13]. The model may thus be written symbolically as

$$\omega+\varrho+(\omega+\varrho)\otimes(P+f)$$

the magnitude of the P and f couplings being taken from fits to πN elastic scattering. This model gives a good account not only of the energy behaviour of the data, but also of the spin and isospin dependence of the amplitudes.

Specifically we write the Regge pole contributions ($R=\omega,\varrho$) to the helicity amplitudes of the appendix (A.6) as

$$f^R_{\mu_2\mu_1\lambda}(s,t)=i(-t)^{\frac{n+x}{2}}\left(\frac{\nu}{\nu_0}e^{-\frac{i\pi}{2}}\right)^{\alpha^R(0)} G^R_{\mu_2\mu_1}e^{c^R_{\mu_2\mu_1}t} \qquad (2.1)$$

with

$$\begin{aligned} c^R_{\mu_2\mu_1} &\equiv a^R_{\mu_2\mu_1}+\alpha'_R\left(\log\frac{\nu}{\nu_0}-\frac{i\pi}{2}\right) \\ x &\equiv |\lambda|+|\mu_1-\mu_2|-n \\ n &\equiv |\lambda-(\mu_1-\mu_2)|, \end{aligned} \qquad (2.2)$$

where $\alpha(t)=\alpha_R(0)+\alpha'_R t$ is the Regge trajectory, G and a are the magnitude and slope parameters of the Regge residue, and $\nu_0=1$ GeV^2 is the usual scale factor, with

$$\nu\equiv\frac{s-u}{2}. \qquad (2.3)$$

The absorbing $P+f$ elastic non-flip amplitude takes the form

$$A(s,t)=i\sigma_T\nu e^{c_P t}+E_0\nu_0\alpha^f(t)e^{c_f t}\left(e^{-\frac{i\pi}{2}}\frac{\nu}{\nu_0}\right)^{\alpha_f(0)}, \qquad (2.4)$$

where

$$\begin{aligned} c_P &\equiv h_P+\alpha'_P\left(\log\frac{\nu}{\nu_0}-\frac{i\pi}{2}\right) \\ c_f &\equiv h_f+\alpha'_f\left(\log\frac{\nu}{\nu_0}-\frac{i\pi}{2}\right) \end{aligned} \qquad (2.5)$$

and the parameters, which are fixed from elastic πN scattering, are listed in Table 1. The $R\otimes(P+f)$ cuts

Table 2. The born term residues

Amplitude	Residue
B_1	$-\frac{g}{2}(F_1+2mF_2)$
B_2	$\frac{g}{2}F_1$
B_3	$\frac{g}{4}F_1$
B_5	0
B_6	$-gF_2$
B_8	$-\frac{g}{2}F_2$

F_1 and F_2 are proton electromagnetic form factors, and g is πNN coupling constant, $g^2/4\pi=14.2$

Table 3. Resonance parameters

Resonance	$l^{\pm}$	Mass	Width	E_l	M_l
S_{11}	0+	1.505	0.1	0.502	0.0
S_{11}	0+	1.688	0.11	0.099	0.0
P_{33}	1+	1.232	0.114	−0.071	3.51
P_{13}	1+	1.850	0.3	0.0	0.0
F_{37}	3+	1.940	0.2	0.014	0.156
P_{11}	1−	1.434	0.2	0.0	0.495
D_{13}	2−	1.514	0.33	0.721	0.269
D_{13}	2−	1.680	0.07	−0.071	0.05
D_{13}	2−	1.971	0.1	0.171	0.036
D_{33}	2−	0.649	0.15	−0.340	0.028
F_{15}	3−	1.682	0.14	0.332	0.113

Note: Mass and width are in GeV/c²
Couplings are in $\mu b^{1/2}$
The transition moments are obtained from Table 1 of [25], multiplying by the appropriate Clebsch-Gordan coefficients to obtain the π° couplings

then have the form

$$f^c_{\mu_2\mu_1\lambda}(s,t) = i\left(\frac{\nu}{\nu_0}e^{-\frac{i\pi}{2}}\right)^{\alpha^R(0)} G^R_{\mu_2\mu_1}(-t)^{\frac{n}{2}}\left[-\frac{\lambda^R_n\sigma_T}{8\pi c_P}\left(\frac{c_P}{c_P+c_R}\right)^{n+1}\right.$$
$$\cdot\exp\left(\frac{c_Rc_Pt}{c_R+c_P}\right)+\alpha^f(0)\left(1+\frac{\alpha'_f}{a_f(0)}\frac{\partial}{\partial c_f}\right)\left(\frac{iE_0\lambda^R_n}{8\pi c_f\nu}\right) \quad (2.6)$$
$$\left.\cdot\left(\frac{c_f}{c_f+c_R}\right)^{n+1}\exp\left(\frac{c_Rc_ft}{c_R+c_f}\right)\left(\frac{\nu}{\nu_0}e^{-\frac{i\pi}{2}}\right)^{\alpha_f(0)}\right]$$

but for $n=0$, $x=2$ the terms $\left(\frac{c_P}{c_P+c_R}\right)^{n+1}$ are replaced by

$$\left[\frac{1}{c_P}\left(\frac{c_P}{c_P+c_R}\right)^2-t\left(\frac{c_P}{c_P+c_R}\right)^3\right].$$

The λ_n are the SCRAM enhancement factors [7, 10].

As reported in [13] this gives an excellent fit to all the data for $p_{lab}>6$ GeV/c, but here, for future convenience, we have changed s to ν, so the parameters of Table 1 are very slightly different from those of [13].

Then using the relationship between these helicity amplitudes and the kinematical singularity free Ball amplitudes [see (A.14)–(A.16) of the Appendix] we evaluate the FESR integrals of these natural parity Regge amplitudes

$$\text{Single-Flip (SF)} = \frac{1}{N}\int_{\nu_T}^{N}\frac{d\nu}{\sqrt{-t'}} \cdot \operatorname{Im}\left(f_{++1}(\nu,t)+f_{--1}(\nu,t)\right)$$
$$\text{Double-Flip (DF)} = \frac{1}{-tN}\int_{\nu_T}^{N} d\nu \operatorname{Im} f_{+-1}(\nu,t) \quad (2.7)$$
$$\text{Non-Flip (NF)} = \frac{1}{N}\int_{\nu_T}^{N} d\nu \operatorname{Im} f_{-+1}(\nu,t),$$

where ν_T is the threshold value of ν, N is the cut-off point which we took to be at $W=2.07$ GeV [see (A.6)]. As the Regge contributions are complicated numerical integration is necessary, and the results are plotted in Fig. 2.

b) The Resonance Integrals

The corresponding integrals over the resonances may be written, from (A.14)–(A.16),

$$\text{SF} = \frac{-\pi\nu_B R_6}{\sqrt{2}N}-\frac{1}{\sqrt{2}N}\int_{\nu_T}^{N}\nu\operatorname{Im}B_6(\nu,t)d\nu$$
$$\text{DF} = \frac{\pi\sqrt{2}R_3}{N}+\frac{\sqrt{2}}{N}\int_{\nu_T}^{N}\operatorname{Im}B_3(\nu,t)d\nu \quad (2.8)$$
$$\text{NF} = \frac{-\sqrt{2}\pi\nu_B}{N}(R_1-mR_6)-\frac{\pi\sqrt{2}tR_3}{N}$$
$$-\frac{\sqrt{2}}{N}\int_{\nu_T}^{N}\nu\operatorname{Im}[B_1(\nu,t)-mB_6(\nu,t)]d\nu$$
$$-\frac{t\sqrt{2}}{N}\int_{\nu_T}^{N}\operatorname{Im}B_3(\nu,t)d\nu$$

where ν_B is the value of ν at $s=m^2$, m being the nucleon mass [see (A.2)], and the R_i are the residues of the nucleon pole listed in Table 2. The main input is the resonance parameters. As we use Devenish and Lyth's parametrization of electroproduction [25] we also employ their Breit-Wigner parameters for the multipoles ($M_{l\pm}$, $E_{l\pm}$)

$$M_{l\pm} = \frac{W_R\Gamma\left(\frac{q_R}{q}\right)^{l+1}}{s_R-s-iW_R\Gamma}M_R \quad (2.9)$$

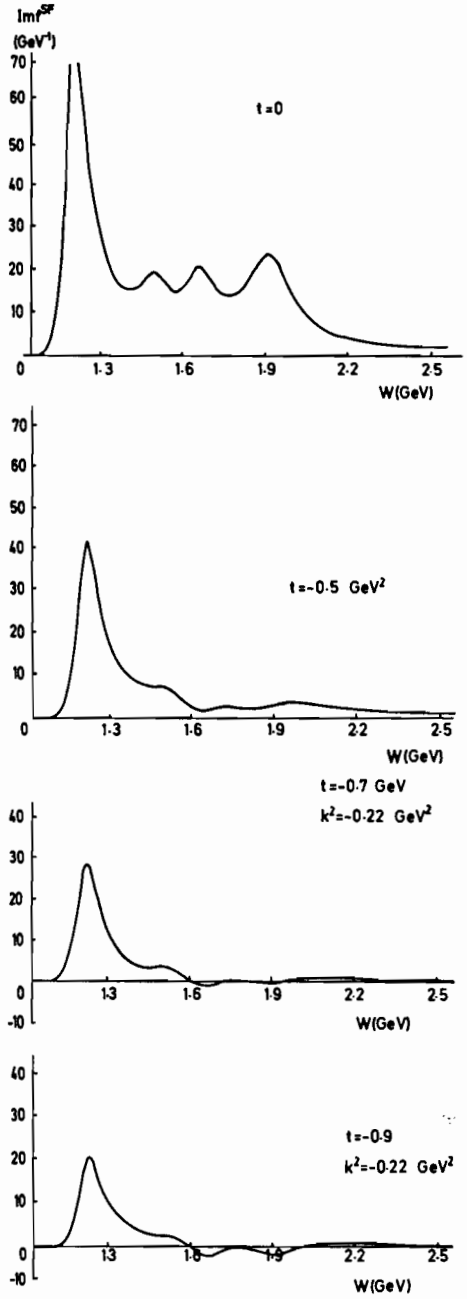

Fig. 3. The resonance contribution to the imaginary part of the single-flip amplitude as a function of W, the centre of mass energy, at selected values of $-t$. The large contribution of the $P_{33}(1236)$ resonance at $-t=0.5$ GeV^2 where one might expect a zero will be noticed. [Remember the integrals in Fig. 2 also include the Born-term contribution in (2.8)]

$$\Gamma=\Gamma_R\left(\frac{q}{q_R}\right)^{2l+1}\left(\frac{q_R^2+X^2}{q^2+X^2}\right)^l \tag{2.10}$$

where $X=0.35$, Γ_R is the resonance width, W_R its mass, q is the πN centre-of-mass momentum and M_R is the multipole coupling.

A more complex parametrization is employed for the $P_{33}(1236)$ multipoles

$$M_{1+}(s)=\frac{kq}{k_R q_R}\,\frac{cq_R^3}{(q_R^2-q^2)(1+q^2a^2)-icq^3}\,M_{P_{33}} \tag{2.11}$$

where k is the photon's momentum, $a^2=21.4$, $C=4.27$, and $q_R=0.2254$, and the electric multipole is given by

$$E_{1+}(s)=(1.19x-0.25)e^{-3x}M_{1+}(s) \tag{2.12}$$

where

$$x\equiv\frac{s-m^2}{2m}-0.15. \tag{2.13}$$

The resonance parameters obtained by Devenish and Lyth [25] are listed in Table 3.

These multipoles may be inserted into Eq. (A.19) to give the CGLN ϕ_i amplitudes, which when inserted into (A.11) give the required Ball amplitudes for (2.8). (Note that the scalar amplitudes do not contribute for photoproduction, $k^2=0$). Thus we can evaluate the resonance FESR by numerical integration.

We have mainly concentrated on the analysis of ref. 25 because it has been extended to electroproduction too. However, it is desirable to try and estimate the uncertainties inherent in these analyses and so we have also evaluated (2.8) using the resonance parameters of Moorhouse et al. [28], and Metcalf and Walker [29]. We find that the differences in the resulting FESR's are generally small (always $<10\%$) and negligible for our purposes.

In each case we used $W=2.07$ GeV as the upper cut off. The results are displayed in Fig. 2. We also attempted to evaluate higher moments in order to check the effective trajectories of the low-energy regime, but it turned out that the integrals were too sensitive to the poorly determined parameters of the fourth resonance region for useful conclusions to be drawn.

c) Comparison of the Two Integrals

Figure 2 shows that the Regge and Resonance FESR, which ought to agree, differ markedly in sign, magnitude and t-dependence in both the non-flip and single-flip amplitudes. Even worse, the expected zero of the single-flip amplitude for $t\simeq-0.5$ GeV^2 has not emerged in either case.

The reason for this as far as the resonances are concerned is apparent if one examines the behaviour of the integrand as a function of t for the dominant single-flip amplitude, (Fig. 3). Most of the resonance contributions do fall to zero $0.3<-t<0.5$ but the dominant $P_{33}(1236)$ does not. This resonance, together

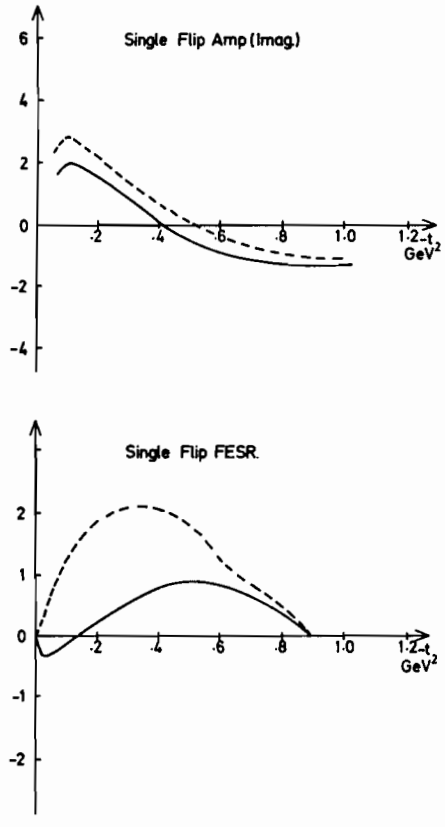

Fig. 4. The shape of the imaginary part of the single flip Regge amplitude at $p_L=6$ GeV/c compared with its FESR (multiplied by $(-t)^{1/2}$ to facilitate the comparison). The full line is the amplitude and the dashed line is the result if the $R\otimes f$ cuts are removed

Table 4. Parameters of the daughter amplitudes used in (2.14)

$\alpha(0)$	−1.71
α'	0.94
G_{++}	−12.4
G_{-+}	17.2
G_{+-}	−0.46
a_{++}	1.64
a_{-+}	1.26
a_{+-}	0.03
b	1.45

with the $D_{13}(1515)$, controls the behaviour of the FESR as the others, and the Born term, are much weaker (see Oderico, [30]). Indeed Armenian et al. [31] have shown that semilocal duality holds in $\gamma p\to\pi^0 p$ except for the P_{33} region. In the corresponding elastic πN amplitudes where semi-local duality is much better, the P_{33} contribution is cancelled by a much stronger nucleon Born term to ensure that the $-t=0.5$ dip is present in the FESR. Odorico suggested that this difference might be due to the different spins occurring in the two processes, but this seems unlikely since $\pi N\to\varrho N$ which is also controlled by ω exchange does have the expected dip [33].

Comparison of the Regge amplitudes at $p_{\text{lab}}=6$ GeV/c with the FESR evaluated over the region up to $W=2.07$ GeV (multiplied by the kinematic factor $(-t)^{n/2}$ in Fig. 4 for ease of comparison) demonstrates that the problem here lies in the continuation to low energy since the Regge amplitudes do have the expected zeros at higher energies even though the FESR do not. It is also clear from Fig. 4 that it is not just our slightly unusual (though necessary) absorption prescription, including the f, which is responsible. Rather the difficulty stems from the fact that the cuts have an unacceptable low-energy behaviour. Indeed it was this observation which led Worden [12] to reject SCRAM models in favour of NWZ models for photoproduction. However since the resonance integrals do not have these zeros either, NWZ models like that of Barker et al. [14] have to employ several Regge-like terms of uncertain physical significance, and only a global not a semi-local duality is achieved.

Since the low energy P_{33} resonance is responsible for most of our problems it seems most reasonable to simulate its effect by adding to our Regge model a daughter trajectory, low lying in the j-plane, which can rectify the mismatch of the Regge and resonance integrals. This was one of the alternatives suggested by Worden [34] in his analysis of duality and absorption, but in his case the anomalous resonance behaviour was not such a problem. It is possible to obtain a very satisfactory fit of both the high-energy data and the FESR's by adding to the Regge amplitudes (2.1) a daughter term with

$$\alpha_d(t)\approx\alpha_\omega(t)-2$$

with the parametrization

$$f_{++}(s,t)=i(-t)^{1/2}\left(\frac{\nu}{\nu_0}e^{-\frac{i\pi}{2}}\right)^{\alpha_d(0)}G^d_{++}e^{c^d_{++}t}(1+bt)$$

$$f_{-+}(s,t)=i\left(\frac{\nu}{\nu_0}e^{-\frac{i\pi}{2}}\right)^{\alpha_d(0)}G^d_{-+}e^{c^d_{-+}t}(\alpha_d+2) \qquad (2.14)$$

$$f_{+-}(s,t)=i(-t)\left(\frac{\nu}{\nu_0}e^{-\frac{i\pi}{2}}\right)^{\alpha_d(0)}G^d_{+-}e^{c^d_{+-}t},$$

where

$$c^d_i=\alpha^d_i+\alpha'_d\left(\log\frac{\nu}{\nu_0}-\frac{i\pi}{2}\right) \qquad (2.15)$$

for $i=++,\ -+$ and $+-$. As this is only an effective singularity factorisation of the residue was not imposed. It was also checked that the resulting amplitudes satisfied semi-local duality. The fit parameters are given in Table 4, and the FESR comparison is shown in Fig. 5.

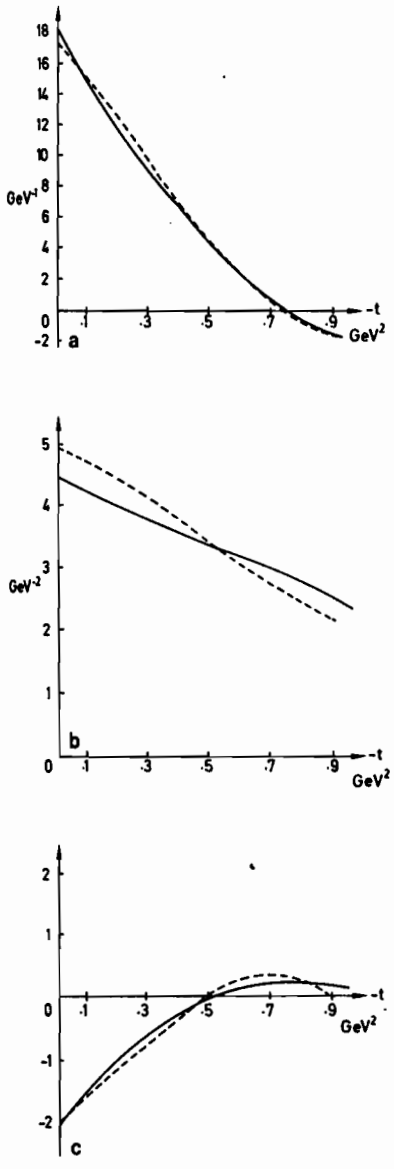

Fig. 5a–c. Fit to the resonance FESR of the Regge model including the daughter term (2.14) with the same conventions as Fig. 2. It will be seen that the agreement is very much improved

Having thus obtained a satisfactory understanding of photoproduction at all energies we must now look at electroproduction.

3. Neutral Pion Electroproduction

a) The Resonance Integral

Since the Ball amplitudes (A.11) are KSF for electroproduction we simply need to know the k^2 dependence of the resonance multipoles in order to extend the analysis of the previous chapter to $k^2 \neq 0$.

Devenish and Lyth [25] write the multipoles in the factorized form.

$$M_{l\pm}(s,k^2) = G(k^2) M_{l\pm}(s), \quad G(0) \equiv 1, \tag{3.1}$$

where $M(s)$ are the Breit-Wigner resonances of (2.9), and the form factors are written as

$$G(k^2) = \prod_{i=1}^{n} \left(1 - \frac{k^2}{k_i^2}\right)^{-1}, \tag{3.2}$$

where

$$k_i^2 \equiv k_1^2 + \frac{i}{n}(k_2^2 - k_1^2) \tag{3.3}$$

with

$$2\mu^2 \leqq k_1^2 \leqq k_2^2 \leqq (m_R + m)^2$$

so k_1 and k_2 are their variable parameters. However, the physical multipoles have kinematical singularities and are subject to threshold contraints (see also [35]). Devenish and Lyth incorporate these by defining (A.22)

$$\phi_\pm \equiv \left[1 - \frac{k^2}{(m_R \pm m)^2}\right]^{1/2} \tag{3.4}$$

and introducing the following combinations:

$$\begin{aligned}
\alpha_{l+} &= \left(\frac{1}{l+1}\right)(lM_{l+} + E_{l+}) = \phi^l \phi_+^{l+1} \bar{\alpha}_{l+} \\
\beta_{l+} &= \left(\frac{1}{l+1}\right)(M_{l+} - (l+2)E_{l+}) = \phi_-^l \phi_+^{l-1} \bar{\beta}_{l+} \\
S_{l+} &= \phi_-^{l+1} \phi_+^l \bar{S}_{l+} \\
E_{l-} &= \phi_+^{l-1} \phi_-^{l-2} \bar{E}_{l-} \\
M_{l-} &= \phi_+^{l-1} \phi_-^l \bar{M}_{l-} \\
S_{l-} &= \phi_+^l \phi_-^{l-1} \bar{S}_{l-}
\end{aligned} \tag{3.5}$$

which are analytic in k^2. But, as noted in the appendix, the scalar multipoles have to satisfy certain constraints at $\phi\pm = 0$, which are accommodated by expressing

$$\begin{aligned}
S_{l+} &= \frac{C|\boldsymbol{k}(m_R, k^2)|}{(k^2 - a)(k^2 - b)} E_{l+}(k^2) \\
S_{l-} &= \frac{C|\boldsymbol{k}(m_R, k^2)|}{(k^2 - a)(k^2 - b)} \frac{1}{l}[M_{l-} - (l-1)E_{l-}],
\end{aligned} \tag{3.6}$$

where

$$b \equiv [3m_R^2 + m^2 - a][1 + a(m_R^2 - m^2)^{-1}]$$

$$c \equiv 2m_R^2[(m_R + m)^2 - a][a - (m_R - m)^2][m_R^2 - m^2 - a]^{-1}$$

and a is a free parameter. Also

$$S_{0+} = \frac{C|k(m_R, k^2)|}{k^2 - a} E_{0+}. \tag{3.7}$$

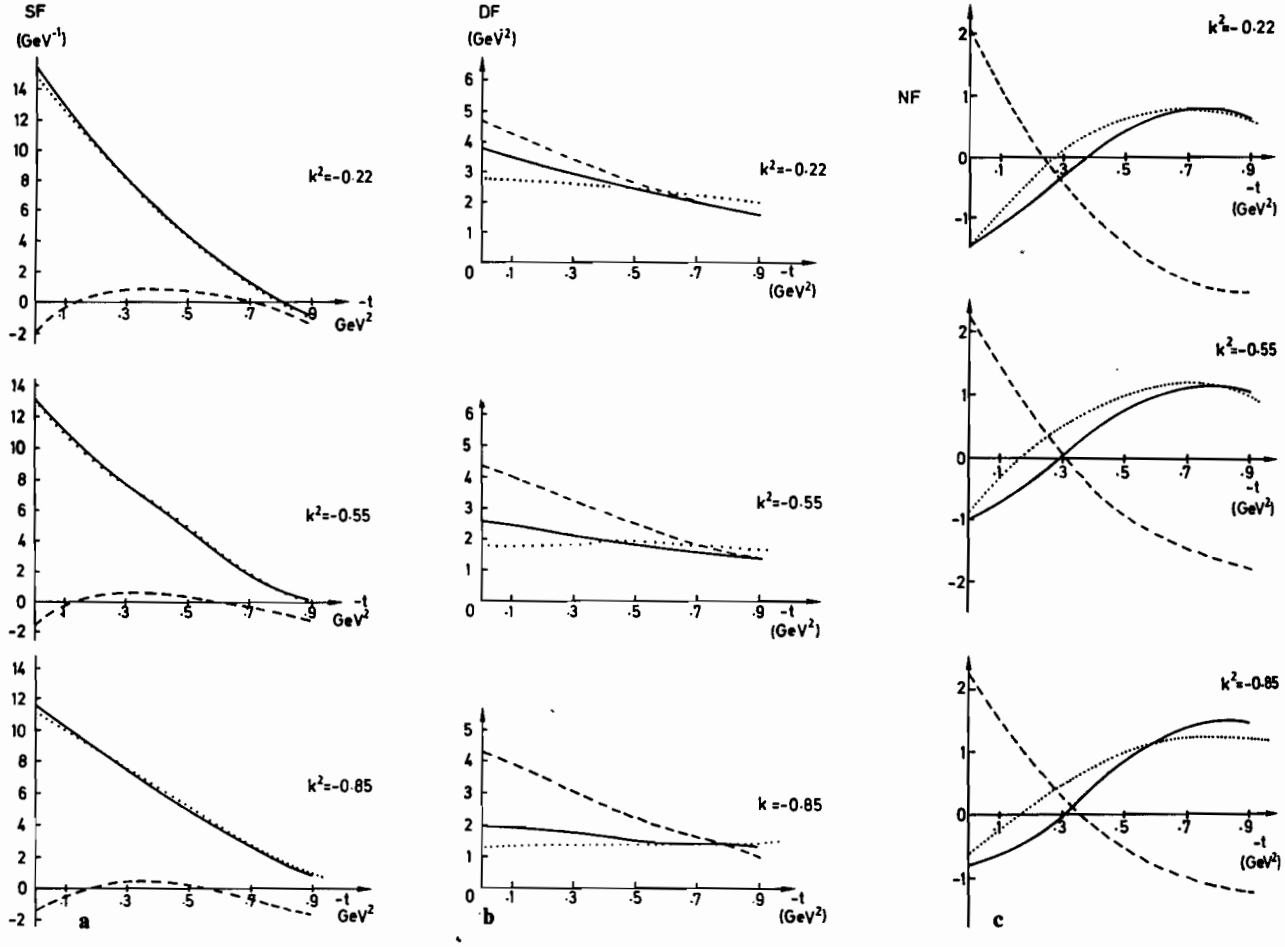

Fig. 6a—c. The results of the electroproduction FESR as a function of t at various valves of k^2 for **a** single-flip, **b** double-flip and **c** non-flip. The dotted line is the resonance FESR, the dashed line is the integral of the Regge model of Sect. 2 plotted to show the k^2 dependance resulting from ν (3.8), while the solid line is the best fit when the k^2 dependence of the daughter (3.10) as well as VDM (3.9) are included

The factor n in (3.2) is related to $\bar{n}$, the asymptotic power of k^{-2} of the multipole, and they set $\bar{n}=3$ for all the resonances except the P_{33} which has $\bar{n}=5$.

We have chosen the recommended fit 4 of Devenish and Lyth [25] whose parameters are listed in Table 5. The FESR resonance integrals of (2.8) were then evaluated at $k^2=-0.22$, -0.55, -0.85 GeV^2 and are displayed in Fig. 6. It will be seen that the magnitude of the integral for the single flip amplitude increases with $-k^2$ for $-t>0.5$ GeV^2. Figure 7 shows that the P_{33} resonance still dominates the integrals.

b) The Regge Integral

The Regge terms are not necessarily functions of k^2. However, we have used the variable [see (A.2)]

$$\nu\equiv\frac{s-u}{2}=s-m^2+\frac{t-\mu^2-k^2}{2} \tag{3.8}$$

which gives rise to a small variation shown in Fig. 6. Also VDM [18] leads us to expect that

$$A^R(s,t,k^2)=\left(1-\frac{k^2}{m_V^2}\right)^{-1}A^R(s,t,k^2=0) \tag{3.9}$$

where m_V is the vector meson mass. Strictly we should use m_ϱ^2 for the ω-exchange term and m_ω^2 for ϱ-exchange, but of course these particles are essentially degenerate. It turns out that our best fit requires $m_V^2\approx 0.6$ (GeV/c^2) very much as expected.

By themselves, however, these modifications are quite insufficient to achieve agreement with the resonance FESR. The problem is that the P_{33} and F_{15} resonances have an anomalous t-dependence whose effect we compensated for in photoproduction by introducing a daughter trajectory. These resonances also have a strong variation of their coupling with k^2, as we noted above, and it therefore semed natural to try and use the daughter term to improve the

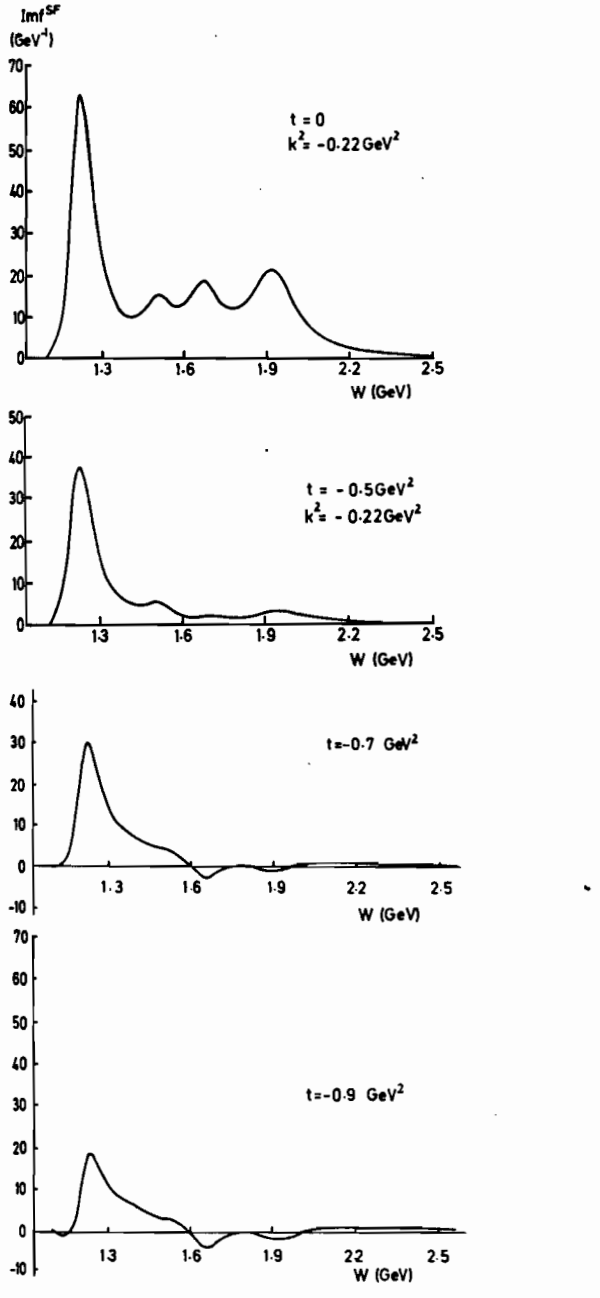

Fig. 7. The resonance contribution to the imaginary part of the single-flip amplitude as a function of W for selected values of $-t$ at $k^2=-0.22$ GeV^2. The large contribution of the $P_{33}(1236)$ is evident

agreement of the electroproduction FESR. We discovered that a simple variation of the magnitude and t dependence of the daughter contribution with k^2, incorporated in the parameterization

$$\begin{aligned} G^d_{++}(k^2)&=G^d_{++}(0)\,(1-g_{++}k^2)\\ a_{++}(k^2)&=a_{++}(0)\;(1+A_{++}k^2)\\ b(k^2)\quad&=b(0)\quad\;(1+Bk^2) \end{aligned}$$

Table 5. Resonance form factor parameters

Resonance	Mass	Multipole	k_1^2	k_2^2	a
S_{11}	1.505	E_{0+}	3.36	4.02	
		S_{0+}			0.09
S'_{11}	1.688	E_{0+}	5.16	5.18	
		S_{0+}			0.04
P_{33}	1.232	α_{1+}	0.545	4.715	
		β_{1+}	0.43	4.715	
		S_{1+}			2.867
P_{13}	1.850	S_{1+}			3.34
F_{37}	1.940	α_{3+}	1.61	4.0	
		β_{3+}	0.11	0.43	
		S_{3+}			0.04
P_{11}	1.434	M_{1-}	0.04	0.041	
		S_{1-}			0.046
D_{13}	1.514	F_{2-}	0.82	1.59	
		M_{2-}	0.9	1.92	
		S_{2-}			2.19
D'_{13}	1.680	E_{2-}	6.85	6.851	
		M_{2-}	0.04	0.045	
		S_{2-}			6.85
D''_{13}	1.971	E_{2-}	0.08	0.25	
		M_{2-}	0.82	2.29	
		S_{2-}			8.46
D_{33}	1.649	E_{2-}	1.09	1.94	
		M_{2-}	4.1	4.12	
		S_{2-}			6.69
F_{15}	1.682	E_{3-}	0.53	1.51	
		M_{3-}	1.14	2.98	
		S_{3-}			6.59

These values are taken from fit 4 of Table 5 of [25]

Table 6. The coefficients of k^2 for the daughter in (3.10). Column (a) gives the values used for the FESR shown in Fig. 6. Column (b) gives the refitted values when the cut is also modified as in (3.11), shown in Fig. 9

	(a)	(b)
g_{++}	2.34	2.38
g_{-+}	1.27	1.26
g_{+-}	4.92	0.506
B	0.919	0.252
A_{++}	0.0	0.886
A_{-+}	0.970	0.649
A_{+-}	47.2	48.1
m_v^2	0.50	0.68
r	–	1.4
H	–	15.25

$$\begin{aligned} G^d_{+-}(k^2)&=G^d_{+-}(0)\,(1-g_{+-}k^2)\\ a_{+-}(k^2)&=a_{+-}(0)\;(1+A_{+-}k^2)\\ G^d_{-+}(k^2)&=G^d_{-+}(0)\,(1-g_{-+}k^2)\\ a_{-+}(k^2)&=a_{-+}(0)\;(1+A_{-+}k^2) \end{aligned} \qquad (3.10)$$

gave the excellent agreement between the two sides of the FESR shown in Fig. 6. The additional parameters are listed in Table 6.

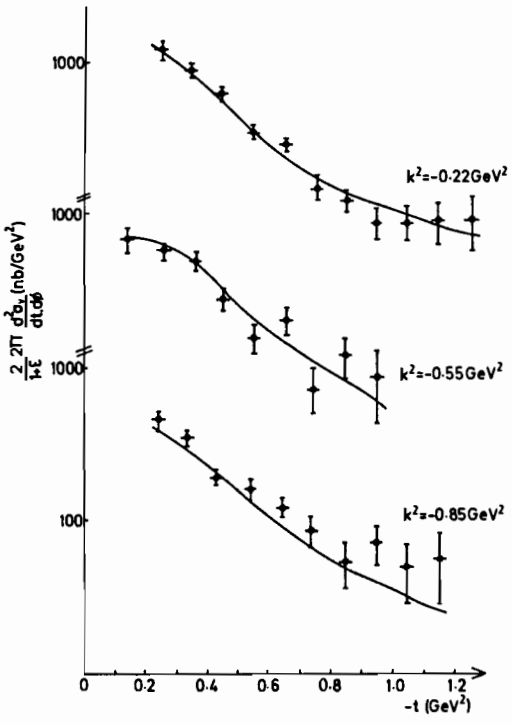

Fig. 8. Fit to the electroproduction differential cross-section including the cut modification (3.11)

It was hoped of course that having thus obtained a parameterization which accords with the FESR for both photoproduction and electroproduction, and with all the data on high-energy photoproduction, we would be able to predict correctly the higher energy electroproduction data and hence begin to understand the disappearance of the dip and secondary maximum in $\frac{d\sigma_V}{dt}$. Such hopes were, however, confounded. The daughter contribution falls rapidly with energy, as of course it must since the old Regge model of [13] fitted high energy photoproduction perfectly well without it. The modest k^2 variations in the leading Reggons incorporated in (3.8) and (3.9) do not remove the dip at $|t|=0.5$ GeV^2 and so our model still contains this dip at all but very low energies.

It was found that only by permitting a rather strong k^2 variation of the Regge cut terms is it possible to obtain an entirely satisfactory fit to all the data. The absorbing $P+f$ amplitude (2.4) is changed by writing

$$\begin{aligned}\sigma_T(k^2)&=\sigma_T(0)\,(1-rk^2)\\ h_P(k^2)&=h_P(0)\,(1-Hk^2)\\ E_0(k^2)&=E_0(0)\,(1-rk^2)\\ h_f(k^2)&=h_f(0)\,(1-Hk^2)\end{aligned}\qquad(3.11)$$

with two new parameters r and H. The parameters of the complete refit are given in Table 6, and the result is illustrated in Figs. 8 and 9. It has a most acceptable $\chi^2/pt=1.05$. [Since it is only the single-flip amplitude which is required to produce the dip an equally good fit can in fact be obtained by incorporating the modification (3.11) only when calculating the absortive corrections to this amplitude, leaving the rest unchanged.]

We attempted many other less drastic modifications of the Regge model of [13], but none proved satisfactory. We conclude that to account simultaneously for the FESR and high-energy data in both photo and electroproduction of π^0's requires a strong cut (SCRAM) type of model with a rather strong k^2 dependence of the cut.

Since the daughter contribution is already very small for $s=6.5$ GeV^2 we do not expect the shape of the electroproduction cross section to change much as one goes to higher energies [though (3.11) does alter the energy dependence of the cut], and the lack of a dip and secondary maximum should be a persistent feature. Some predictions are shown in Fig. 10.

This is quite contrary to the conclusion of Vanryckegem [23] who removed the dip by including a daughter trajectory which cancelled the NWZ dip of the ω at low energies. The residues and slope of this daughter had a rather strange dependence on k^2, however. He predicted that the dip should reappear for $s>12$ GeV^2 and that the electroproduction cross section will be very similar in shape to photoproduction at higher energies. Barker and Storrow [24] tried to explain the data by allowing a modification of the cut contribution with k^2 in a model with NWZ, but they were not able to understand the very rapid transition between $k^2=0$ and $k^2=-0.22$ GeV^2 which they likewise attributed to low-energy effects. We have found a good fit with a SCRAM model in which the main features of the electroproduction data at $s=6.5$ GeV^2 are expected to persist at higher energies.

4. Conclusion

The electro-production data really demand a SCRAM explanation. It is quite clear from Fig. 1 that the low t region ($|t|<0.5$ GeV^2) and the high t region ($|t|>0.5$ GeV^2) of $\frac{d\sigma}{dt}$ have quite different k^2 dependences. Only a model in which these two regions are dominated by different exchanges can give a natural explanation of such a behaviour. In the SCRAM model the low $|t|$ regime is Regge pole dominated, and here the only important k^2 dependence is the factor $\left(1-\frac{k^2}{m_V^2}\right)^{-1}$ pre-

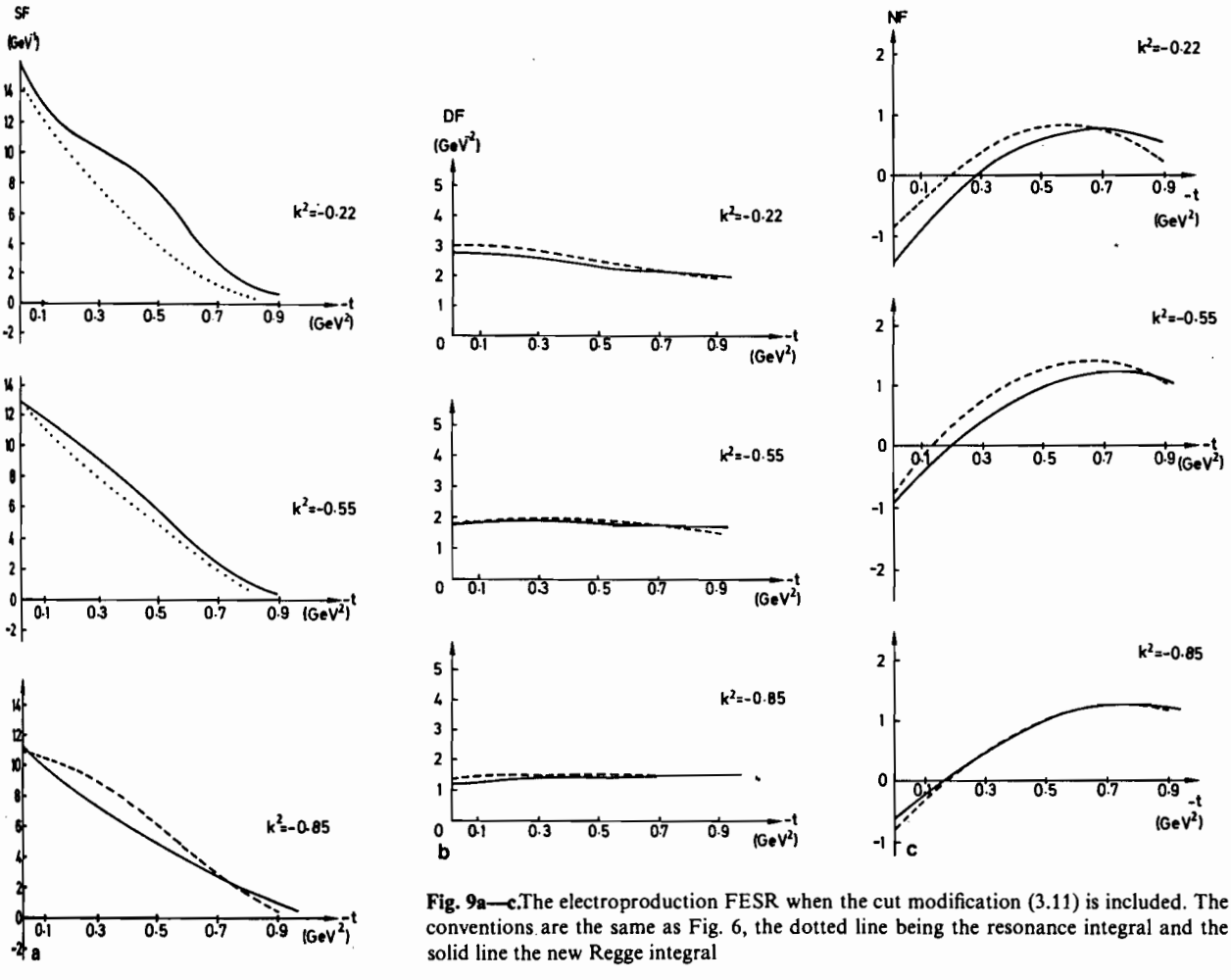

Fig. 9a—c. The electroproduction FESR when the cut modification (3.11) is included. The conventions are the same as Fig. 6, the dotted line being the resonance integral and the solid line the new Regge integral

dicted by VDM. But the large $|t|$ region of the dominant single-flip amplitude is controlled by the Regge cut, and the rapid variation of the cut magnitude with k^2 from (3.11) is rather remarkable. We have found that this is the only straightforward way of accounting for the data. Giving a k^2 dependence to the poles, or changing only the strength but not the t-dependence of the cuts, is quite unable to explain what is observed.

Superficially our change of the cut term with k^2 is similar to that of Irving [36] for charged pion photoproduction who found that a cut of the form

$$C(t,k^2)=(1-0.48\,k^2)G_c \exp\,[(1+0.13\,k^2)at] \qquad (4.1)$$

explained the data. For electroproduction, where $k^2<0$, the cut strength increases and the slope of the t dependence decreases. Irving related this to the transition from a hadron-like photon for $k^2\approx m_\varrho^2$ to a more point-like scaling coupling in deep inelastic scattering where $k^2\ll 0$ (see also [37]). Note that his $C(k^2)\sim k^2$ is very different from Harari's $C(k^2)\sim -k^{-2}$ in (1.2). We too have found that the cut strength must increase linearly with k^2 in (3.11), but the magnitude of the effect is some 3 times greater than in charged pion photoproduction.

But the more significant difference between our results and those of Irving is that the sign of the change of the t dependence with k^2, represented by H in (3.11), is opposite to that of (4.1) so that the width of our cut in t decreases, and decreases very rapidly, with k^2. This means that the absorption is occurring at larger impact parameters the larger is $-k^2$. The shape of the single-flip amplitude as a function of impact parameter is shown in Fig. 11 in which it will be seen that whereas for photoproduction we have the usual peripheral peak at $b\approx 1$ *fm*, the peak is larger and much further out for $k^2<0$, well beyond the spatial extension of a non-interacting baryon.

This behaviour is quite contrary to the expected decrease of the distance travelled by the hadronic fluctuations of the photon as $-k^2$ increases expressed by (1.2). This decrease is supposed to mark the approach to the scaling, pointlike region of k^2, and to

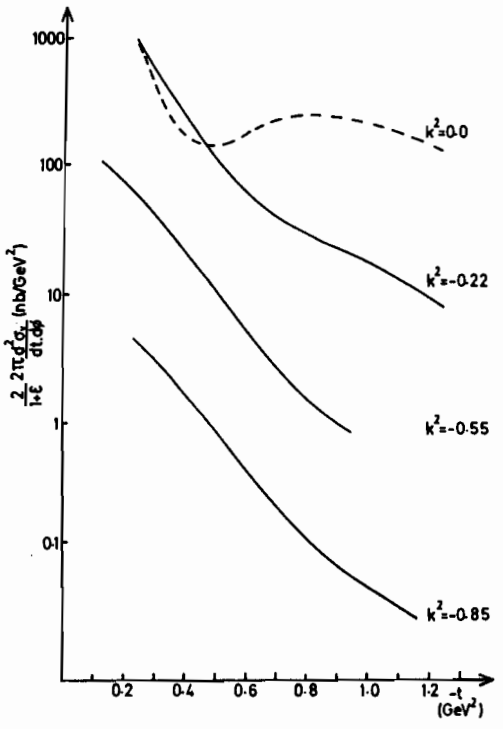

Fig. 10. The predicted electroproduction cross-section at $p_L=12$ GeV/c for various values of k^2. Photoproduction ($k^2=0$) is shown for comparison

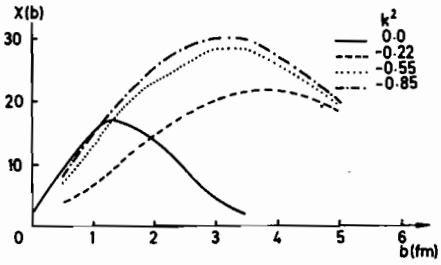

Fig. 11. The impact parameter profile of the single-flip amplitude in our fit to the photoproduction and electroproduction data at $p_L=6$ GeV/c. The rapid change of shape as a function of k^2 is evident

account for the lack of shadowing found in virtual-photon-nucleus scattering [38]. It would seem therefore that the Regge cut region is quite separate from the scaling region. This is also the case in pp elastic scattering [39, 40] where the dip at $|t|=1.4$ GeV^2, followed by a secondary maximum, is due to the presence of an almost imaginary $P\otimes P$ cut which interferes with the P pole, and is quite distinct from the (real) scaling region $|t|>3$ GeV^2, where [42]

$$\frac{d\sigma}{dt}\sim s^{-n}f(\cos\theta). \tag{4.2}$$

Thus unfortunately it appears that it is wrong to suppose that the behaviour of the Regge cuts must anticipate the approach to scaling. This is perhaps not too surprising if one considers Fig. 12. Figure 12a shows the VDM Regge coupling, and when squared as in Fig. 12b could also contribute in the scaling region "handbag" diagram of Fig. 12c leading to the proton's valence quark structure function taking the form [41]

$$F(x)\underset{x\to 0}{\sim}x^{1-\alpha(0)} \tag{4.3}$$

Ordinary planar absorption diagrams could also contribute in this limit. However a proper Regge cut diagram, with the "double cross" structure of Fig. 12d [7], requires that the struck parton should interact again with the hadron. It is generally supposed that such diagrams will not contribute in the scaling region since this fast parton is travelling in the opposite direction to the hadron (in the parton's Breit frame). The cut should thus die away as $-k^2$ is increased, perhaps exposing again the endpoints of the Regge poles given by Fig. 12c, as in the constituent interchange model [42].

We conclude that $\gamma_V(k^2)p\to\pi^0 p$, like $\gamma p\to\pi^0 p$ analysed in [13], requires a SCRAM type of model not a NWZ model if all aspects of the data are to be understood. This to some extent justifies Harari's belief [9] that these processes might permit a crucial test of Regge cut models. However, contrary to the very reasonable expectations of many authors, the effective range of

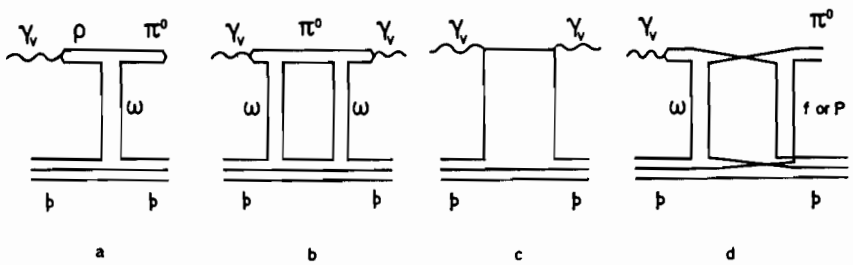

Fig. 12. a Quark line diagram for $\gamma_v p\to\pi^0 p$ via Regge pole exchange in the vector domenance model. **b** The square of (**a**) which contributes to; **c** the "handbag" diagram for deep inelastic scattering; **d** Quark line diagram for a Regge cut with the "double-cross" structure

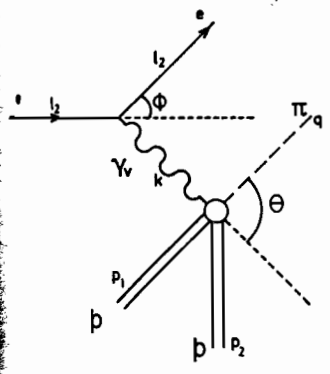

Fig. 13. The kinematics of $ep \to ep\pi^\circ$

this component of the photon-proton interaction increases with $-k^2$, producing a cut which falls more rapidly with $-t$. This has nothing to do with the pointlike scaling behaviour of the $\gamma_V p$ interaction at larger $-k^2$ which arises from quite different parton-model diagrams from those which are expected to contribute to the Regge cuts. The decrease of the Regge cut contribution ensures dominance of the scaling "handbag" diagram at large $-k^2$. Only in this way can one account for the fact that whereas Regge theory expects amplitudes to become more and more complicated as $-t$ is increased with a superposition of multi-Reggeon exchange cuts, QCD predicts a rather simple, almost scaling behaviour at large momentum transfers.

Appendix

Electroproduction Kinematics and Amplitudes

We have gathered into this appendix the main formulae which we use to relate the Regge pole helicity amplitudes and resonance multipole moments to the kinematical singularity free invariant amplitudes which are needed to write FESR. Most of these results may be found in [44], but we repeat them here because they are essential if the reader is to follow the calculations we have made.

We label the four-momenta of the particles as in Fig. 13, and define

$$\begin{aligned} s_T &= (l_1+p_1)^2 \\ t &= (l_1-l_2)^2 \\ s &= (k+p_1)^2 = W^2 \\ t &= (k-q)^2 = \mu^2 + k^2 + 2k^0 E_\pi - 2|\boldsymbol{k}|\,|\boldsymbol{q}|\cos\theta, \\ u &= (k-p_2)^2 \end{aligned} \tag{A.1}$$

where μ is the pion mass and $\cos\theta$ is angle between the incident photon and the scattered pion.

$$\nu = \frac{s-u}{2} = k\cdot(p_1+p_2) = 2k^0 W - k^2 + \frac{t-\mu^2-k^2}{2}$$

$$= W^2 - m^2 + \frac{t-\mu^2-k^2}{2}, \tag{A.2}$$

where m is the mass of the proton.

The electroproduction differential cross section is [43, 44]

$$\frac{d\sigma}{dk^2 d\phi ds dt} = (2^{14}\pi^4 m^3 E_L^2 k_L)^{-1} \sum_{\text{spins}} |T|^2, \tag{A.3}$$

where ϕ is the electrons scattering angle in the laboratory frame, E_L is its incident laboratory frame energy and k_L is the photon's laboratory frame energy. We use centre of mass helicity amplitudes $f_{\mu_2\mu_1\lambda}$ for the photon-proton interaction so that

$$\begin{aligned} \frac{1}{4}\Sigma|T|^2 = \frac{e^2}{k^2}\,\frac{1}{\varepsilon-1}\,\{&|f_{++1}|^2 + |f_{+-1}|^2 + |f_{-+1}|^2 + |f_{--1}|^2 \\ &+ 2\varepsilon(|f_{++0}|^2 + |f_{-+0}|^2) \\ &- 2\varepsilon\,\mathrm{Re}\,(f_{++1}f^*_{--1} - f_{+-1}f^*_{-+1})\cos 2\phi \\ &- 2\sqrt{\varepsilon(\varepsilon+1)}\cos\phi\,(f_{++1}f^*_{+0} - f_{++0}f^*_{--1} \\ &+ f_{+-1}f^*_{-+0} + f_{-+0}f^*_{+-1})\}, \end{aligned} \tag{A.4}$$

where the polarization parameter ε is given by

$$\varepsilon^{-1} = 1 - 2\,\frac{|\boldsymbol{k}_L|}{k^2}\tan^2\frac{\phi}{2} \tag{A.5}$$

and as usual we have used $\pm$ for $\pm\frac{1}{2}$.

For photoproduction, in which the photon has helicity ± 1 only, the differential cross section is

$$\begin{aligned} \frac{d\sigma_\gamma}{dt} = 0.3893\ &[2^5\pi(s-m^2)^2]^{-1} \\ &\cdot\{|f_{++1}|^2 + |f_{+-1}|^2 + |f_{-+1}|^2 + |f_{--1}|^2\} \end{aligned} \tag{A.6}$$

and from this we define the virtual photon differential cross section to be

$$\frac{d\sigma_v}{dt} = 0.3893\ [2^5\pi(s-m^2)^2]^{-1}\ \{''\}, \tag{A.7}$$

where the term in brackets $\{\ \}$ is the same as in (A.4) above.

Comparing this with (A.3) we have

$$\frac{d\sigma}{dk^2 d\phi ds dt} = \Gamma\,\frac{d\sigma_v}{dt}, \tag{A.8}$$

where

$$\Gamma \equiv (s-m^2)\,[2^6\pi^3 m^2 E_L^2(1-\varepsilon)]^{-1}\,(e^2/-k^2) \tag{A.9}$$

is the conventional factor relating electroproduction and photoproduction cross sections.

The helicity amplitudes are related to the CGLN amplitudes [45] ϕ_i by

$$
\begin{aligned}
f_{++1} &= \sqrt{2}\sin\frac{\theta}{2}\left\{\phi_1+\phi_2+\cos^2\frac{\theta}{2}(\phi_3+\phi_4)\right\}\\
f_{--1} &= -\sqrt{2}\sin\frac{\theta}{2}\cos^2\frac{\theta}{2}(\phi_3+\phi_4)\\
f_{+-1} &= \sqrt{2}\sin^2\frac{\theta}{2}\cos\frac{\theta}{2}(\phi_3-\phi_4)\\
f_{-+1} &= -\sqrt{2}\cos\frac{\theta}{2}\left\{\phi_1-\phi_2-\sin^2\frac{\theta}{2}(\phi_3-\phi_4)\right\}\\
f_{++0} &= \frac{k}{|k|}\cos\frac{\theta}{2}(\phi_5+\phi_6)\\
f_{-+0} &= \frac{k}{|k|}\sin\frac{\theta}{2}(\phi_5-\phi_6).
\end{aligned}
\tag{A.10}
$$

The first two of these are single-flip amplitudes, f_{+-1} is the double flip and f_{-+1} the non-flip amplitude. The last two occur only in electroproduction. (Note that a factor $8\pi W$ connects our ϕ_i to the conventional $\mathscr{F}_i$ of CGLN.)

The Ball amplitudes [46] $B_i(s,t)$, $i=1\ldots8$, are kinematical singularity free (KSF) invariant amplitudes for electroproduction. They are related to the ϕ_i by

$$
\begin{aligned}
B_1 &= \frac{1}{2W}\left\{\frac{\phi_1}{z_1z_2}-\frac{\phi_2}{y_1y_2}\right\}\\
B_2 &= \frac{1}{4W^2|k|^2}\left\{(s-m^2-k^2)k^2B_1-2mk^2B_5\right.\\
&\quad+\left(k^0\frac{\mu^2-k^2-t}{2}-k^2E_\pi\right)\\
&\quad\cdot\left[\frac{(W+m)\phi_4}{z_1z_2y_2}-\frac{(W-m)\phi_3}{y_1y_2z_2^2}\right]\\
&\quad\left.+k^2\left[\frac{(W+m)\phi_6}{z_1y_2}-\frac{(W-m)\phi_5}{y_1z_2}\right]\right\}\\
B_3 &= \frac{B_2}{2}+\frac{1}{2W}\left\{\frac{(W-m)\phi_3}{y_1y_2z_2^2}-\frac{(W+m)\phi_4}{z_1z_2y_2^2}\right\}\\
B_5 &= -\frac{1}{2W}\left\{\frac{(W+m)\phi_1}{z_1z_2}+\frac{(W-m)\phi_2}{y_1y_2}\right\}\\
B_6 &= \frac{1}{2W^2|k|^2}\left\{-2mk^2B_1+(s-m^2-k^2)B_5\right.\\
&\quad+\left(k^0\frac{\mu^2-k^2-t}{2}-k^2E_\pi\right)\\
&\quad\cdot\left(\frac{\phi_3}{y_1y_2z_2^2}+\frac{\phi_4}{z_1z_2y_2^2}\right)+k^2\left(\frac{\phi_5}{y_1z_2}+\frac{\phi_6}{z_1y_2}\right)\Big\}\\
B_8 &= \frac{1}{2}B_6-\frac{1}{2W}\left\{\frac{\phi_3}{y_1y_2z_2^2}+\frac{\phi_4}{z_1z_2y_2^2}\right\},
\end{aligned}
\tag{A.11}
$$

where we have introduced

$$
\begin{aligned}
z_1 &\equiv (E_1+m)^{1/2} \quad z_2 \equiv (E_2+m)^{1/2}\\
y_1 &\equiv (E_1-m)^{1/2} \quad y_2 \equiv (E_2-m)^{1/2}.
\end{aligned}
\tag{A.12}
$$

Note that B_4 and B_7 do not appear because of current conservation which requires that

$$
\begin{aligned}
2k^2B_4 &= (t-k^2-\mu^2)B_3-\frac{s-u}{2}B_2\\
k^2B_7 &= B_5-\frac{s-u}{4}B_6+\frac{t-k^2-\mu^2}{2}B_8
\end{aligned}
\tag{A.13}
$$

It is the amplitudes (A.11) for which dispersion relations and hence FESR may be written.

They are related to the helicity amplitudes in terms of which our Regge model is parametrized by [47]

Single Flip

$$
\begin{aligned}
f_{++1}+f_{--1} &= \sqrt{2}\sin\frac{\theta}{2}(\phi_1+\phi_2)\\
&= \left(\frac{-t}{2|q|\,|k|}\right)^{1/2}\left\{z_1z_2\left[(W-m)B_1-B_5\right)\right]\\
&\quad -y_1y_2\left[(W+m)B_1+B_5\right]\}\\
&\sim -\sqrt{\frac{-t}{2}}\,\nu B_6.
\end{aligned}
\tag{A.14}
$$

Double flip:

$$
\begin{aligned}
f_{+-1} &= \sqrt{2}\cos\frac{\theta}{2}\sin^2\frac{\theta}{2}(\phi_3-\phi_4)\\
&= \frac{-t}{2\sqrt{2}}\left\{\frac{z_2}{z_1}\left[2B_3-B_2+(W+m)\left(\tfrac{1}{2}B_6-B_8\right)\right]\right.\\
&\quad\left.+\frac{y_2}{y_1}\left[2B_3-B_2-(W-m)\left(\tfrac{1}{2}B_6-B_8\right)\right]\right\}\\
&\sim \frac{-t}{2\sqrt{2}}\left\{4B_3-B_2+2m\left(\tfrac{1}{2}B_6-B_8\right)\right\}.
\end{aligned}
\tag{A.15}
$$

Non-flip:

$$
\begin{aligned}
f_{-+1} &= \sqrt{2}\cos\frac{\theta}{2}\left\{-(\phi_1-\phi_2)\right\}+f_{+-}\\
&\sim -\sqrt{2}\,\nu(B_1-mB_6)-t\sqrt{2}B_3.
\end{aligned}
\tag{A.16}
$$

The high-energy Regge behaviour of these amplitudes is

$$
\begin{aligned}
B_1,\ B_2,\ B_6,\ B_8 &\sim s^{\alpha-1}\\
B_3,\ B_5 &\sim s^{\alpha}.
\end{aligned}
\tag{A.17}
$$

The crossing properties of these amplitudes under $s\to u$ for $\gamma p\to\pi^0 p$ are

$$
\begin{aligned}
B_i(\nu) &= B_i(-\nu) \quad \text{for} \quad i=1,2,6\\
B_i(\nu) &= -B_i(-\nu) \quad \text{for} \quad i=3,5,8.
\end{aligned}
\tag{A.18}
$$

Finally the ϕ_i amplitudes are related to the electric, magnetic and scalar resonance transition amplitudes by [45]

$$\phi_1 = 8\pi W \sum_l [lM_{l+} + E_{l+}] P'_{l+1}(z) + [M_{l-}(l+1) + E_{l-}] P'_{l-1}(z)$$

$$\phi_2 = 8\pi W \sum_l [M_{l+}(l+1) + lM_{l-}] P'_l(z)$$

$$\phi_3 = 8\pi W \sum_l [E_{l+} - M_{l+}] P''_{l+1}(z) + [E_{l-} + M_{l-}] P''_{l-1}(z)$$

$$\phi_4 = 8\pi W \sum_l [M_{l+} - E_{l+} - M_{l-} - E_{l-}] P''_l(z) \qquad \text{(A.19)}$$

$$\phi_5 = 8\pi W \sum_l (l+1) S_{l+} P'_{l+1}(z) - lS_{l-} P'_{l-1}(z)$$

$$\phi_6 = 8\pi W \sum_l [lS_{l-} - (l+1) S_{l+}] P'_l(z).$$

It is these transition amplitudes which form the basis of our evaluation of the resonance FESR. Note that since the B_i are KSF Eqs. (A.11) and (A.19) imply that these transition amplitudes have kinematical singularities and are subject to constraints at the threshold and pseudo-threshold values of $k^2 = (m_R \pm m)^2$ [25]. This is because the factors in (A.12) may be written

$$(E_l \pm m)^{1/2} = \frac{(W \pm m)}{\sqrt{2W}} \left[1 - \frac{k^2}{(W \pm m)^2}\right]^{1/2}, \qquad \text{(A.20)}$$

$$\xrightarrow[W \to m_R]{} \frac{m_R \pm m}{\sqrt{2m_R}} \phi_\pm, \qquad \text{(A.21)}$$

where

$$\phi_\pm \equiv \left[1 - \frac{k^2}{(m_R \pm m)^2}\right]^{1/2} \qquad \text{(A.22)}$$

vanishes for $k^2 = (m_R \pm m)^2$, i.e. at the threshold or pseudo-threshold in k.

References

1. Frautschi, S.C.: Phys. Rev. Lett. **17**, 722 (1966)
2. Barger, V., Phillips, R.J.N.: Phys. Lett. **53** B, 195 (1974)
3. Arnold, R.C., Blackmon, M.L.: Phys. Rev. **176**, 2082 (1968)
4. Henyey, F., Kane, G.L., Pumplin, J., Ross, M.H.: Phys. Rev. **182**, 1579 (1969)
5. Kane, G.L., Seidl, A.: Rev. Mod. Phys. **48**, 309 (1976)
6. Harari, H.: Ann. Phys. **63**, 432 (1971)
7. Collins, P.D.B.: Regge theory and high energy physics. Cambridge: Cambridge University Press 1977
8. Irving, A., Worden, R.P.: Phys. Rep. **34**, 117 (1977)
9. Harari, H.: Phys. Rev. Lett. **27**, 1028 (1971)
10. Ross, M., Henyey, F., Kane, G.L.: Nucl. Phys. B**23**, 269 (1970)
11. Gault, F.D., Martin, A.D., Kane, G.L.: Nucl. Phys. B**32**, 429 (1971)
12. Worden, R.P.: Nucl. Phys. B**37**, 253 (1972)
13. Collins, P.D.B., Fitton, A.: Nucl. Phys. B**68**, 125 (1974)
14. Barker, I., Donnachie, A., Storrow, J.: Nucl. Phys. B**79**, 431 (1974)
15. Cheng, H., Wu, T.T.: Phys. Rev. **183**, 1324 (1969)
16. Bjorken, J.D., Kogut, J.B., Soper, D.E.: Phys. Rev. D**3**, 1382 (1971)
17. Donnachie, A., Shaw, G.: Electromagnetic interaction of hadrons, Vol. 2. A. Donnachie, C. Shaw (eds.). New York, London, Plenum Press 1978
18. Sakurai, J.J.: Ann. Phys. **11**, 1 (1960)
19. Frass, H., Read, B.J., Schildknecht, D.: Nucl. Phys. B**86**, 346 (1975)
20. Wolf, G., Soding, P.: Electromagnetic interactions of hadrons, Vol. 2. A. Donnachie, G. Shaw (eds.). New York, London: Plenum Press 1978
21. Brasse, F.W. et al.: Nucl. Phys. B**58**, 467 (1975)
22. Berger, Ch. et al.: Nucl. Phys. B**137**, 1 (1978)
23. Vanryckeghen, L.G.F.: Neutral pion electroproduction at intermediate and high energies. Liverpool University Report (1976, unpublished)
24. Barker, I., Storrow, J.: Nucl. Phys. B**135**, 285 (1978)
25. Devenish, R.C.E., Lyth, D.H.: Nucl. Phys. B**93**, 109 (1975)
26. Moorhouse, R.G.: Proceedings of EPS international conference on high energy physics. A. Zichichi (ed.), Palermo, Bologna: Editori Compositori 1975
27. Close, F.E., Gilman, F.J.: Phys. Lett. **38** B, 541 (1972)
28. Moorhous, R.G., Oberlack, H., Rosenfeld, A.H.: Phys. Rev. D**9**, 1 (1974)
29. Metcalf, W.J., Walker, R.L.: Nucl. Phys. B**76**, 253 (1974)
30. Odorico, R.: Nucl. Phys. B**101**, 480 (1975)
31. Armenian, H.K. et al.: Phys. Rev. D**12**, 1278 (1975)
32. Michael, W., Gidal, G.: Phys. Rev. Lett. **28**, 1475 (1972)
33. Haber, B. et al.: Phys. Rev. D**10**, 1387 (1974)
34. Worden, R.P.: Nucl. Phys. B**58**, 205 (1973)
35. Devenish, R.C.E., Eisenschitz, T., Korner, J.G.: Phys. Rev. D**14**, 3063 (1976)
36. Irving, A.C.: Nucl. Phys. B**86**, 125 (1975)
37. Collins, P.D.B., Fitton, A.: Nucl. Phys. B**91**, 332 (1975)
38. Grammar, G., Sullivan, J.: Electromagnetic interactions of hadrons, Vol. 2. A. Donnachie, G. Shaw (eds.). New York, London: Plenum Press 1978
39. Collins, P.D.B., Gault, F.D., Martin, A.: Nucl. Phys. B**85**, 141 (1975)
40. Collins, P.D.B., Gault, F.D.: Physics Lett. **73** B, 330 (1978)
41. Close, F.E.: An introduction to quarks and partons. New York: Academic Press 1979
42. Sivers, D., Brodsky, S.J., Blankenbecler, R.: Phys. Rep. **23** C, 1 (1976)
43. Dombey, N.: Rev. Mod. Phys. **41**, 236 (1969)
44. Lyth, D.H.: Electromagnetic interactions of hadrons, Vol. 1. A. Donnachie, G. Shaw (eds.). New York, London: Plenum Press 1978
45. Chew, G.F., Goldberger, M.L., Low, F.E., Nambu, Y.: Phys. Rev. **106**, 1345 (1957)
46. Ball, J.S.: Phys. Rev. **124**, 2014 (1961)
47. Ball, J.S., Jacob, M.: Nuovo Cimento **54** A, 620 (1968)

Responsible for advertisements: L. Siegel, Kurfürstendamm 237, D-1000 Berlin 15. Telephone: (030) 8821031, Telex: 01-85411 – Springer-Verlag Berlin · Heidelberg · New York
Printer: Brühlsche Universitätsdruckerei, Giessen – Printed in Germany

Dieses Heft enthält eine Beilage des Springer-Verlages Berlin Heidelberg New York